Monthly Notices of the ROYAL ASTRONOMICAL SOCIETY

MNRAS **510,** 3132–3144 (2022) https://doi.org/10.1093/mnras/stab3453
Advance Access publication 2021 November 27

Red supergiants in M31: the Humphreys–Davidson limit at high metallicity

Sarah L. E. McDonald [1]★ Ben Davies[1] and Emma R. Beasor[2]†

[1]*Astrophysics Research Institute, Liverpool John Moores University, Liverpool Science Park ic2, 146 Brownlow Hill, Liverpool L3 5RF, UK*
[2]*NSF's NOIRLab, 950 N Cherry Ave, Tucson, AZ 85719, USA*

Accepted 2021 November 24. Received 2021 November 24; in original form 2021 July 20

ABSTRACT

The empirical upper limit to red supergiant (RSG) luminosity, known as the Humphreys–Davidson (HD) limit, has been commonly explained as being caused by the stripping of stellar envelopes by metallicity-dependent line-driven winds. As such, the theoretical expectation is that the HD limit should be higher at lower metallicity, where weaker mass-loss rates mean that higher initial masses are required for an envelope to be stripped. In this paper, we test this prediction by measuring the luminosity function of RSGs in M31 and comparing it to those in the LMC and SMC. We find that $\log(L_{\rm max}/{\rm L}_\odot) = 5.53 \pm 0.03$ in M31 ($Z \gtrsim {\rm Z}_\odot$), consistent with the limit found for both the LMC ($Z \sim 0.5\ {\rm Z}_\odot$) and SMC ($Z \sim 0.25\ {\rm Z}_\odot$), while the RSG luminosity distributions in these three galaxies are consistent to within 1σ. We therefore find no evidence for a metallicity dependence on both the HD limit and the RSG luminosity function, and conclude that line-driven winds on the main sequence are not the cause of the HD limit.

Key words: stars: evolution – stars: massive – supergiants.

1 INTRODUCTION

It is well established that there is an empirical upper limit to red supergiant (RSG) luminosity (Stothers 1969; Sandage & Tammann 1974), often referred to as the 'Humphreys–Davidson (HD) limit' (Humphreys & Davidson 1979). The HD limit is often explained as being a manifestation of mass-loss (e.g. Humphreys & Davidson 1979) during the lifetime of a star, caused by strong stellar winds or episodic periods of mass-loss, where the fraction of mass lost from the stellar envelope is dependent on the initial mass of the star. Under this explanation, lower initial mass supergiants (∼8–15M$_\odot$) experience winds that are not strong enough to remove the entire hydrogen envelope on the main sequence (MS, Maeder 1981; Maeder & Meynet 2003) so the star is able to evolve to the RSG phase, where it resides before dying as a core-collapse supernova. Higher initial mass stars (∼15–30M$_\odot$) can lose a considerable fraction of their envelope, causing the star to undergo only a brief RSG phase before evolving to a Wolf–Rayet (WR) star (Stothers & Chin 1979). At even higher masses ($\gtrsim$ 30M$_\odot$), the entire envelope can be lost by the time hydrogen in the core is exhausted, preventing evolution to the cool red side of the Hertzsprung–Russell (HR) diagram. These stars instead evolve directly from the MS to a WR star, completely bypassing the RSG phase (Stothers & Chin 1978). Under this scenario, the HD limit therefore represents the luminosity corresponding to the most massive star that may still experience an RSG phase.

Massive stars lose mass both on the MS and during the RSG phase. Beasor et al. (2020) show that the contribution of mass-loss from cool RSG winds is extremely small, where the total mass lost is only expected to be in the range of 1–2M$_\odot$. This means that quiescent mass-loss during the RSG phase is not effective at removing a significant fraction of the hydrogen envelope prior to core collapse.

In terms of the proposed explanation of the HD limit, this then places more emphasis on mass-loss from either luminous blue variable (LBV)-type eruptions, discussed further in Section 4.3.1, or line-driven winds during the hot MS phase (Castor, Abbott & Klein 1975; Vink, de Koter & Lamers 2001). These line-driven winds are produced by absorption of photospheric photon momentum by UV metal lines (Kudritzki 2003), and it therefore follows that there could be a metallicity dependence with radiatively driven wind strength whereby decreased metallicity results in decreased wind strength (Abbott 1982; Kudritzki, Pauldrach & Puls 1987). For these reasons, evolutionary models predict that lower-metallicity environments should produce more luminous supergiants due to this dependence of mass-loss on metallicity (Maeder & Meynet 2003). This means that the HD limit should therefore also be metallicity dependent.

The HD limit has been measured previously in the literature, the first being a hard upper limit of $\log(L/{\rm L}_\odot) = 5.8 \pm 0.1$ inferred by Humphreys & Davidson (1979), using an optically selected sample of cool supergiants in the Milky Way and the Large Magellanic Cloud (LMC). This was later revised to $\log(L/{\rm L}_\odot) = 5.66$ in Humphreys (1983). Davies et al. (2018, hereafter DCB18) revisited the HD limit in the Magellanic Clouds, with more complete samples and higher-precision multiwavelength photometry, finding an upper limit of $\log(L/{\rm L}_\odot) = 5.5$ for both the Small Magellanic Cloud (SMC) and the LMC.

★ E-mail: S.E.McDonald@2015.ljmu.ac.uk
† Hubble Fellow.

© 2021 The Author(s)
Published by Oxford University Press on behalf of Royal Astronomical Society

Downloaded from https://academic.oup.com/mnras/article/510/3/3132/6445032 by Liverpool John Moores University user on 09 May 2022

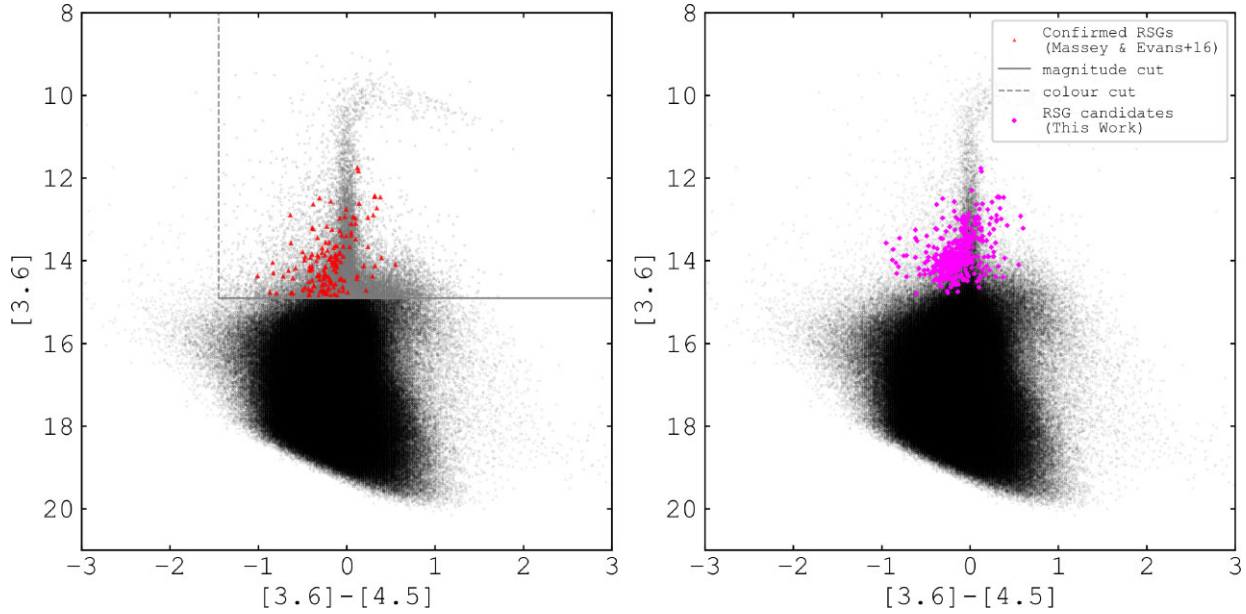

Figure 1. (a) A colour–magnitude diagram, where the black points in both panels indicate all the M31 point sources detected by *Spitzer* IRAC/MIPS (Khan 2017). The grey points show the sources that fit the criteria to be likely RSG candidates based on the colour (dashed grey line) and magnitude (solid grey line) cuts applied, to find the first constraint towards establishing a sample of RSG candidates. The red triangles indicate known M31 RSGs with determined spectral classifications by ME16 which we have based our colour and magnitude cuts on. All other mid-IR cuts can be seen in Table 1. (b) The magenta points indicate all the RSG candidates (with available *Spitzer* mid-IR photometry) that we find and use in the present work after all photometric and astrometric cuts have been applied.

To study the HD limit at higher metallicity, the most obvious environment would be the Milky Way. However, there are a number of obstacles in studying the RSG population of the Milky Way, such as high foreground extinction and uncertain distances. Therefore, only an incomplete luminosity distribution of RSGs in the Galaxy is achievable, although Davies & Beasor (2020) argue that, even with an effective sample size of over 100, there are still no RSGs with luminosity greater than $\log(L/L_{\odot}) = 5.5$ in the Galaxy, and conclude that the HD limit at solar metallicity is comparable to that of the SMC and LMC. However, studies of stellar populations in the plane of the Milky Way will always be subject to criticisms of completeness. Therefore, to investigate the HD limit at high metallicity, a similar galaxy-wide study to that of DCB18 is required, but in a higher-metallicity galaxy.

In this paper, we complement the study of DCB18 with an investigation into the Humphreys–Davidson limit of M31. Our close proximity to M31 (0.77 Mpc, Karachentsev et al. 2004) gives us the ability to study resolved stellar populations at high metallicity, which is thought to be in the range of $1.05–1.66 Z_{\odot}$ (Zurita & Bresolin 2012). The work in this current paper is distinct from other recent studies of the RSG population of M31 (e.g. Massey & Evans 2016; Gordon, Humphreys & Jones 2016; Neugent et al. 2020; Massey et al. 2021) in that we focus on the high-luminosity end of the RSG luminosity function and the HD limit as well as make quantitative comparisons with RSG populations in lower-metallicity galaxies.

2 COMPILING THE SAMPLE

To compile a sample of RSG candidates in M31, we use photometry from the *Spitzer* mid-infrared point-source survey (IRAC/MIPS: 3.6, 4.5, 5.8, 8.0, and 24 μm) from Khan (2017). RSGs tend to be bright in the mid-infrared as a result of their relatively low temperatures. They also experience strong stellar winds, which can produce quantities of dust that can obscure stars at optical wavelengths. Therefore, any particularly dusty or 'dust-enshrouded' stars (van Loon et al. 2005) may be too faint to be detected by optical or possibly even near-IR surveys. Additionally, at these longer wavelengths there is less sensitivity to interstellar reddening. By using the Khan catalogue as a basis, we expect to have a much higher level of completeness than can be achieved from optical or near-IR surveys (we discuss sample completeness further in Section 3.4).

2.1 Method

To locate our target stars, we first constructed colour–magnitude diagrams (CMDs) using the *Spitzer* photometry (Khan 2017); see Fig. 1. Next, we overplotted a sample of known RSGs from Massey & Evans (2016, hereafter ME16), to define the location of our target stars in mid-IR colour–magnitude space. We place a colour threshold at the blue limit of known RSGs in M31, as well as a magnitude cut corresponding to $\log(L/L_{\odot}) \sim 4.8$ to avoid any asymptotic giant branch stars (AGBs) or red giants contaminating our sample (Ferrari et al. 1970; Lamb, Iben & Howard 1976; Brunish, Gallagher & Truran 1986). The colour–magnitude cuts are listed in Table 1. In addition to this, we made a radius cut at 40 kpc (with a dust-free exponential disc of scale length $R_{\rm d} = 5.3 \pm 5$ kpc, Courteau et al. 2011), using the physical deprojected radius, assuming an inclination angle of 77.5° (Tempel, Tamm & Tenjes 2010).

Next we cross-matched our candidates with the RSG catalogues from ME16 and Gordon et al. (2016, hereafter GHJ16) to ensure that all the brightest candidates from these optical surveys had been reacquired through our mid-IR cuts. We found 10 objects with $\log(L/L_{\odot}) > 5$ from ME16 and 14 from GHJ16 that do not appear in the Khan catalogue (the reasons for which are discussed in Section 3.1), which are then manually added in to our sample of RSG candidates. This results in a sample of 7893 RSG candidates so

Downloaded from https://academic.oup.com/mnras/article/510/3/3132/6445032 by Liverpool John Moores University user on 09 May 2022

Table 1. The *Spitzer* colour and magnitude cuts that were applied to locate our target stars. The cuts are based on the colours and magnitudes of known confirmed RSGs from ME16.

Spitzer magnitudes (IRAC/MIPS)	Magnitude cut (mag)
IRAC1 (3.6 μm)	14.9
IRAC2 (4.5 μm)	15.0
IRAC3 (5.8 μm)	14.8
IRAC4 (8.0 μm)	14.8
MIPS1 (24 μm)	12.8
Spitzer colours (IRAC/MIPS)	Colour cut (mag)
[3.6]–[4.5]	−1.45
[3.6]–[5.8]	−1.3
[3.6]–[8.0]	−1.0
[5.8]–[8.0]	−0.6
[3.6]–[24]	0.0
[8.0]–[24]	0.0
[4.5]–[24]	0.4

far. These stars are then cross-matched to the following catalogues to obtain multiwavelength photometry and astrometry for each candidate:

(i) Local Group Galaxy Survey (LGGS) *UBVRI* photometry (Massey et al. 2006).

(ii) *Gaia* EDR3 photometry (BP and RP bands) and astrometry (proper motion and parallax) (Gaia Collaboration 2020).

(iii) Two Micron All Sky Survey (2MASS) *JHK* photometry (Cutri et al. 2003).

After coadding the optical/near-IR photometry, we applied an extra colour criteria of *Gaia* BP − RP > 1 to further screen out any objects that are too blue in colour to be RSGs.We then also use *Gaia* astrometry as a method of removing foreground stars. We aim for as high a completion rate as possible, so we remove any objects with a proper motion deviating more than 4σ from the motion of M31 (Salomon et al. 2020), to exclude foreground objects from our sample. The combination of these additional *Gaia* cuts removes a large number of foreground and blue objects from our sample. The total number of RSG candidates found and used in this work is 415. We discuss the completeness of our RSG sample in Section 3.4.

2.2 Correcting for foreground extinction

Since we do not have associated spectroscopic information for all of these RSG candidates, we cannot correct for extinction using intrinsic colours. Furthermore, the colours of RSGs are often affected by circumstellar extinction, which unlike interstellar extinction does not reduce the observed bolometric flux (see Section 3.1). For these reasons, we must obtain an estimate of the foreground extinction separately. To do this we utilize an M31 extinction map (Dalcanton et al. 2015), surveyed by the Panchromatic Hubble Andromeda Treasury project (PHAT, Dalcanton et al. 2012). This provides a foreground extinction correction, A_V, for any of our RSG candidates that are situated within the north-east quadrant of M31. Each RSG candidate was then dereddened according to the Cardelli, Clayton & Mathis (1989) reddening law for the optical photometry, and Rieke & Lebofsky (1985) for the near-IR.

The candidates that are located outside the PHAT footprint cannot be individually extinction corrected. For these stars, we adopt the median A_V of the 149 RSGs that are covered by PHAT. The middle panel of Fig. 2 shows the visual extinction A_V of these stars as a function of their bolometric luminosities (our method of determining bolometric luminosity is discussed in Section 3.1). From the median and the 68 per cent probability limits, we determine an average $A_V = 1.19 \pm 0.10$.

To investigate whether the assumption of using a uniform A_V for the stars not covered by PHAT introduces any systematics into our results, we determine the bolometric luminosity of the 149 candidates using both their individual A_V from the extinction map and the median $A_V = 1.19$. The top panel of Fig. 2 shows the number of objects in each bin of the luminosity function when using both the average uniform A_V and the individual PHAT extinction corrections. Though the exact number of objects in each bin is different, the two are consistent to within the Poisson errors. Furthermore, L_{max} is the same whichever extinction correction method is used. Therefore, we conclude that the assumption of a uniform A_V results in a luminosity distribution and L_{max} that are stable to within the error margin.

3 LUMINOSITY DISTRIBUTIONS AND L_{MAX}

3.1 Determining bolometric luminosities

We converted the dereddened photometry into fluxes using Vega-calibrated zero-point fluxes for each filter from the SVO Filter Profile Service (Rodrigo & Solano 2020). Using these fluxes, we plot spectral energy distributions (SEDs) for each RSG candidate and integrate under the SED to determine bolometric luminosity, using the IDL routine `int_tabulated`, adopting an M31 distance modulus of 24.4 (Karachentsev et al. 2004). In doing so, we make the same assumption as DCB18 that any flux lost to absorption by circumstellar material is reradiated at longer wavelengths, and so by integrating under the SED from the optical to the mid-IR we obtain all of the star's flux. Fig. 3 shows the SEDs of the most luminous candidates with complete photometry from the optical to the mid-IR. In Section 3.3, we discuss in more detail the brightest RSG candidates as well as any bright objects that were rejected from our sample.

A few of the objects in our sample have incomplete photometric coverage, often due to them being undetected at longer wavelengths. These objects were identified when comparing the sample of stars found in the present work with previously compiled M31 RSG catalogues (ME16; GHJ16), where we found that 24 stars with $\log(L/L_\odot) > 5$ were missed from our study. *Spitzer*/IRAC and MIPS images[1] of these objects show that they appear to be spatially extended in the mid-IR, and as a result are absent from the Khan (2017) point-source catalogue. To estimate the luminosities of these objects, we employ an alternative method of using a *K*-band bolometric correction (BC_K), which we describe below.

3.2 Bolometric corrections

In this section, we use the RSGs with complete photometric coverage to determine bolometric corrections (BCs) appropriate for M31. We use *K*-band photometry since a BC_K at this wavelength does not appear to be sensitive to spectral type (DCB18). Furthermore, the extinction at this wavelength is only around a tenth of that in the *V* band. The bolometric correction is then used to estimate luminosities for the stars with incomplete SED coverage.

We individually deredden the near-IR photometry, prior to converting to bolometric luminosity by employing either (a) a uniform $A_K = 0.13 \pm 0.02$ found from the median $A_V = 1.19 \pm 0.1$ and the

[1] *Spitzer* images were taken from the NASA/IPAC Infrared Science Archive.

Downloaded from https://academic.oup.com/mnras/article/510/3/3132/6445032 by Liverpool John Moores University user on 09 May 2022

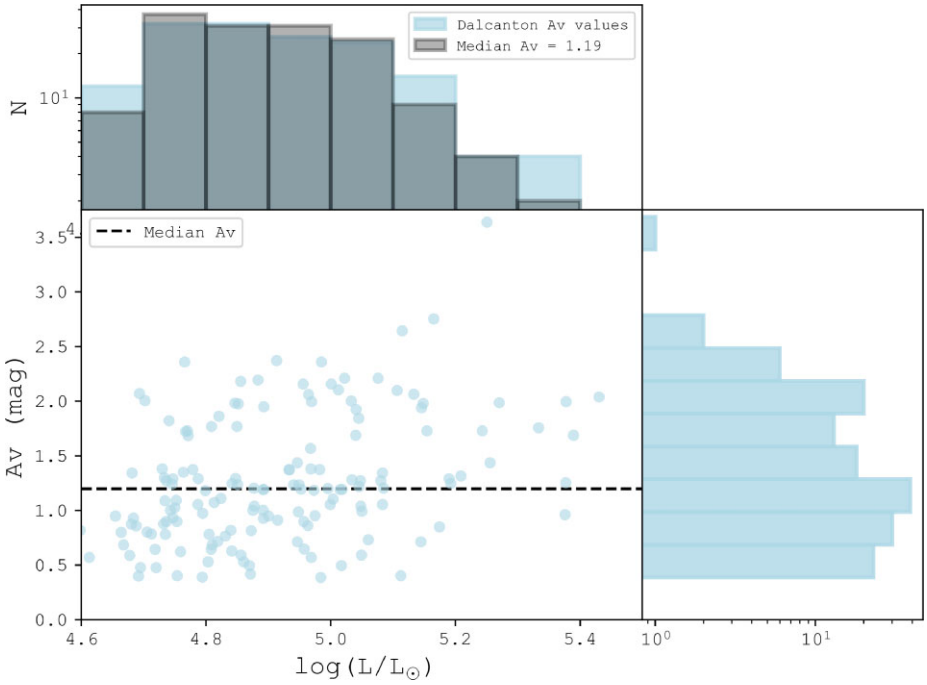

Figure 2. Top: A luminosity distribution of the 149 RSG candidates found in the region of M31 surveyed by *HST* PHAT (Dalcanton et al. 2012). The luminosities in light blue are determined using A_V taken directly from the Dalcanton et al. (2015) M31 extinction map. The grey distribution is the same stars but with their luminosities determined using $A_V = 1.19 \pm 0.10$, which corresponds to the median of all the RSGs located within the PHAT-surveyed region. Middle: Bolometric luminosity versus A_V of 149 RSG candidates present in the M31 extinction map. Right: A distribution of the visual extinction values for each star, taken from the extinction map.

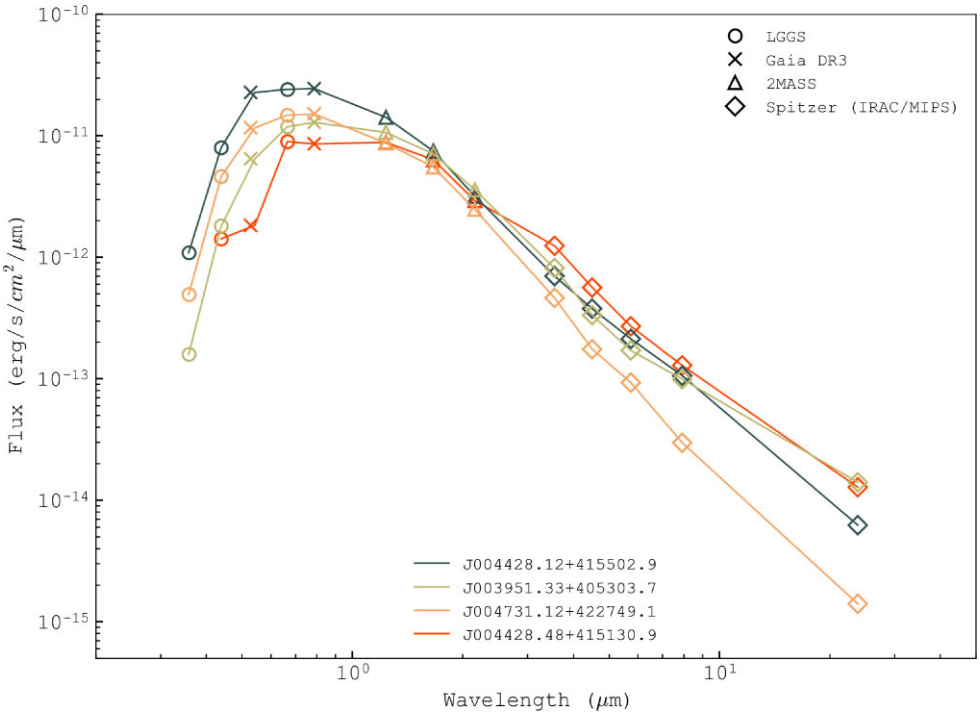

Figure 3. Spectral energy distributions of the most luminous red supergiant (RSG) candidates. These have $\log(L/L_\odot) > 5.4$ with complete dereddened photometry ranging from the optical through to the mid-infrared. The symbols in the upper legend indicate the catalogue source of the photometry and the lower legend provides the LGGS star name for each candidate. Each of these luminous RSGs is discussed in more detail in Section 3.3.

Downloaded from https://academic.oup.com/mnras/article/510/3/3132/6445032 by Liverpool John Moores University user on 09 May 2022

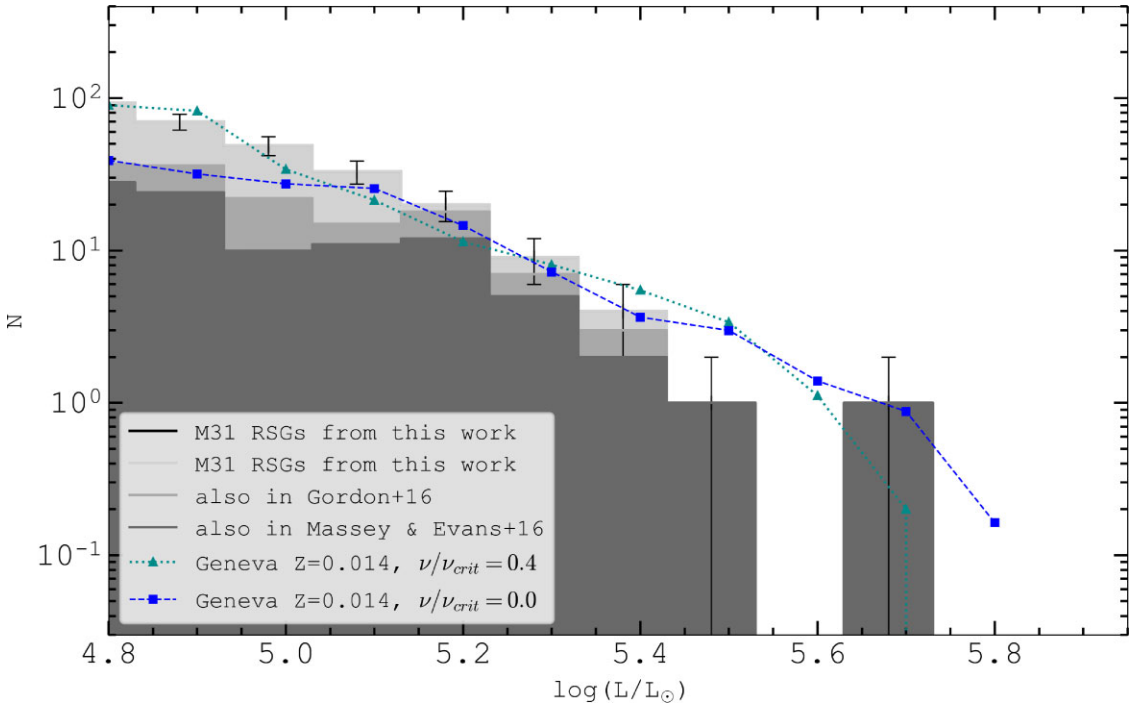

Figure 4. The red supergiant luminosity distribution for M31. The observed luminosity distribution from this work is shown in light grey, with the two darker-grey distributions showing the number of RSG candidates that we use in this study that are also found in previous M31 RSG studies. Overplotted are the rotating ($v/v_{\rm crit} = 0.0$) and non-rotating ($v/v_{\rm crit} = 0.4$) model-predicted distributions from the Geneva models at solar metallicity ($Z = 0.014$) from Ekström et al. (2012). Note that the brightest star at $\log(L/L_\odot) = 5.71$ cannot be definitively ruled out, but is a borderline M31 candidate due to its proper motion. This is discussed further in Section 3.3.

relation $A_K = 0.11A_V$ from Rieke & Lebofsky (1985); or (b) the individual A_V if situated in the extinction map and finding A_K using the same A_V/A_K relation. We then calculate BC by finding $M_{\rm BOL} - M_\lambda$ for each of our RSG candidates; see Fig. 4. We find the median $BC_K = 2.71 \pm 0.12$ as well as $BC_{\rm IRAC1} = 3.18 \pm 0.15$, where the uncertainty is the standard deviation. We also plot a binned average of BC_λ with $M_{\rm BOL}$ to show that within the uncertainties there is no systematic trend with brightness.

The BC_K that we find for M31 is consistent with those found in previous studies for other Local Group galaxies. There is good agreement with the median BC across spectral classes K and later derived for the LMC, with a median BC of 2.81 ± 0.08, and the SMC, with 2.60 ± 0.09, both from DCB18, as well as 2.81 ± 0.10 for the Milky Way, from Davies & Beasor (2018).

3.3 The most luminous RSG candidates in M31

The most important candidates for our investigation into the HD limit are those occupying the high end of the luminosity function. The photometric and astrometric constraints implemented, previously discussed in Section 2, ensure that the stars in our sample have the appropriate colours, magnitudes, and proper motion consistent with being RSG candidates in M31. However, only approximately 25 per cent of the sample has spectroscopic confirmation. This means that there may be some contamination. Therefore, a further verification step that we applied was to inspect high spatial resolution archival images such that all objects at the bright end of the luminosity function ($\log(L/L_\odot) > 5.3$) are consistent with being single sources.

The observational luminosity function of M31 RSGs is shown in Fig. 5 by the light-grey distribution. It shows the number of RSG candidates per log luminosity bin for M31, found in the present work. The two darker-grey distributions show the number of RSG candidates that we use in this study that are also found in previous M31 RSG studies. For the brightest RSGs, their luminosities and spectral classifications can be seen in Table 2. Below are the most luminous candidates discussed in more detail.

(i) **J004520.67+414717.3**: This object has previously been assigned a spectral classification of M1I with a luminosity of $\log(L/L_\odot) = 5.81$ by ME16 and $\log(L/L_\odot) = 5.94$ by GHJ16. In the present work, we determine a luminosity of $\log(L/L_\odot) = 5.75 \pm 0.11$. This makes this object the brightest RSG candidate that we find in M31. However, there are some caveats to the significance of this high-luminosity object in regard to $L_{\rm max}$. First, although this object has optical colours consistent with RSGs ($B - V = 2.68$ and $V - R = 1.55$), the source appears to be located within spatially extended infrared emission, meaning that it does not appear in the Khan point-source catalogue. As a result its luminosity is determined using a BC_K where the large uncertainty is dominated by that on the bolometric correction. Further, this candidate has a proper motion that deviates from the M31 proper motion at the 2σ level. This raises the possibility that it is a foreground object, which is also suggested in ME16, as they find the radial velocity of this object overlaps foreground star velocities. This casts further uncertainty on its luminosity as the M31 distance assumed in the luminosity calculation is no longer appropriate if it is not an M31 member. Since we cannot definitively rule out this object since it has an RSG classification, it remains in our sample. However, we will treat this object with caution in regard to the HD limit.

(ii) **J004428.12+415502.9**: This candidate has been previously classified as a K2I RSG from ME16 with a luminosity of $\log(L/L_\odot) = 5.64$, as well as a luminosity of $\log(L/L_\odot) = 5.89$ from GHJ16. It has

Downloaded from https://academic.oup.com/mnras/article/510/3/3132/6445032 by Liverpool John Moores University user on 09 May 2022

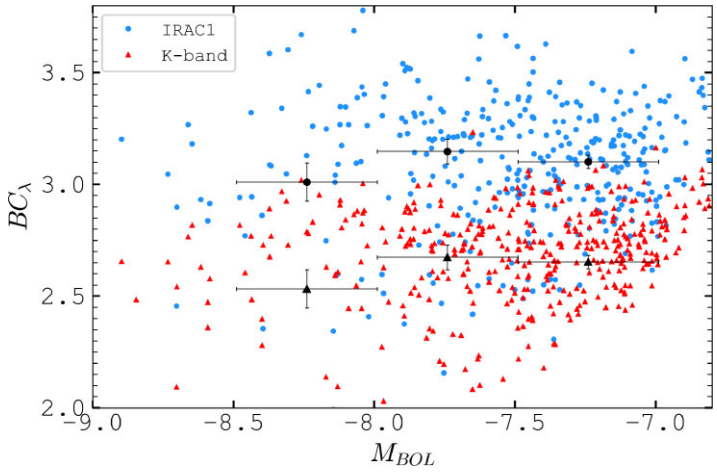

Figure 5. The offset $M_{\rm BOL} - M_\lambda$ is used to estimate the bolometric correction for each RSG candidate in both the *K* band, seen in red, and the IRAC1 3.6 μm band, in blue.

Table 2. The name, position, and bolometric luminosity of the RSG candidates with $\log(L/{\rm L}_\odot) > 5.4$ found in this study. We also provide the SIMBAD object classification of each candidate, assigned by either Massey et al. (2009) or ME16. Full analyses of these objects and their luminosities are described in Section 3.3. ∗The uncertainty of these luminosities is dominated by the error on the BC_K, discussed further in Section 3.1.†This is our borderline candidate, which has been previously classified as an M1I supergiant; our caveats for this objects are discussed in Section 3.3.

LGGS name	RA, Dec. (J2000)	$\log(L/{\rm L}_\odot)$	Classification
J004520.67+414717.3	$00^{\rm h}45^{\rm m}20\overset{\rm s}{.}66$, $+41^\circ47'17\overset{''}{.}1$	5.75 ± 0.11∗	RSG (M1I)†
J004428.12+415502.9	$00^{\rm h}44^{\rm m}28\overset{\rm s}{.}11$, $+41^\circ55'02\overset{''}{.}7$	5.53 ± 0.03	RSG (K2I)
J004539.99+415404.1	$00^{\rm h}45^{\rm m}39\overset{\rm s}{.}98$, $+41^\circ54'03\overset{''}{.}9$	5.49 ± 0.09∗	RSG (M3I)
J003951.33+405303.7	$00^{\rm h}39^{\rm m}51\overset{\rm s}{.}32$, $+40^\circ53'03\overset{''}{.}6$	5.46 ± 0.02	'Possible' RSG
J004731.12+422749.1	$00^{\rm h}47^{\rm m}31\overset{\rm s}{.}04$, $+42^\circ27'48\overset{''}{.}2$	5.44 ± 0.04	'Possible' RSG
J004428.48+415130.9	$00^{\rm h}44^{\rm m}28\overset{\rm s}{.}47$, $+41^\circ51'30\overset{''}{.}7$	5.43 ± 0.02	RSG (M1I)

also been described as a long-period variable candidate in Soraisam et al. (2018) in their study of RSG variability in M31. We initially found a luminosity of $\log(L/{\rm L}_\odot) = 5.63$, but closer inspection of SDSS images shows it to be two blended stars of similar colour. The brighter of the two stars has astrometry consistent with M31, but the fainter has a high proper motion and is therefore likely to be a foreground object. From the ratio of the two stars' fluxes, we estimate that the M31 star has an apparent brightness 0.1 dex greater than the foreground star. This leads to a revised brightness for the RSG of $\log(L/{\rm L}_\odot) = 5.53 \pm 0.03$.

(iii) **J004539.99+415404.1**: This star is classified as an M3I RSG with a luminosity of $\log(L/{\rm L}_\odot) = 5.81$ in ME16 and $\log(L/{\rm L}_\odot) = 6.09$ in GHJ16. In the present work, we initially calculated a luminosity of $\log(L/{\rm L}_\odot) = 5.81$ from its SED, but in *HST* images and in *Gaia* DR3 we find that the object resolves into two sources. One source has no *Gaia* astrometry but the other has a large detectable proper motion in *Gaia* DR3, indicating foreground membership.The two sources also have comparable brightnesses and colours at *Gaia* BP and RP wavelengths (the RSG candidate has BP − RP = 2.389 475, the nearby red object BP − RP = 2.389 486). We have full SED coverage for this object, but the derived luminosity will consequently contain flux contributed from both sources in the near and mid-IR, which results in an overestimation of the object's luminosity. Under the assumption that the star with no astrometry is an M31 member, and that the stars are of comparable apparent brightness at all wavelengths, we use the 2MASS *K*-band photometry (which detects these objects as only one source) and allocate a *K*-band flux to the RSG that is half of the total *K*-band flux. We then use a *K*-band BC to determine its luminosity, which we find to be $\log(L/{\rm L}_\odot) = 5.49 \pm 0.09$.

(iv) **J003951.33+405303.7**: This candidate has been previously identified as a 'possible RSG' in Massey et al. (2009), but has not been spectroscopically confirmed. This object has optical colours consistent with RSGs and in SDSS images appears as a single object for which we find a luminosity of $\log(L/{\rm L}_\odot) = 5.46 \pm 0.02$. This object also passed our proper-motion constraint of deviating less than 4σ from the proper motion of M31, consistent with M31 membership. We find no reason to exclude this object based on its high-resolution images; therefore it remains in our sample.

(v) **J004731.12+422749.1**: This object is a 'possible RSG' according to GHJ16, with a luminosity of $\log(L/{\rm L}_\odot) = 5.53$, but has not been spectroscopically confirmed. This object passed our proper-motion cuts and is therefore presumed to be an M31 member. In the present work, we determine a luminosity of $\log(L/{\rm L}_\odot) = 5.44 \pm 0.04$ and find no reason to reject this object, so it remains in our sample.

(vi) **J004428.48+415130.9**: This is another confirmed RSG with a spectral type of M1I and a previously determined luminosity of $\log(L/{\rm L}_\odot) = 5.60$ by ME16 and $\log(L/{\rm L}_\odot) = 5.64$ by GHJ16. The *Gaia* proper motions of this object are consistent with the proper motion of M31, so we presume that this object is an M31 member. Lastly, this star appears to be a single object in *HST* images for which we find a luminosity of $\log(L/{\rm L}_\odot) = 5.43 \pm 0.02$ from its SED.

Downloaded from https://academic.oup.com/mnras/article/510/3/3132/6445032 by Liverpool John Moores University user on 09 May 2022

3.3.1 Stars rejected from this work

The following objects are those that met both our colour and magnitude criteria and have $\log(L/L_\odot) > 5.3$, but were rejected after inspecting their high-resolution images. The reasons for rejection are described below:

(i) **J004257.58+411740.1**: Our initial estimate of this star's luminosity was $\log(L/L_\odot) = 5.81$. However, despite having both mid-IR and optical colours consistent with RSGs, this object is located within the bulge of M31 where there is little to no star formation occurring, making it unlikely to be a massive star. Also, the object appears spatially extended in *HST B*-band images, consistent with the object being a globular cluster, which is also suggested by Wirth, Smarr & Bruno (1985). Therefore, we reject this object from our sample.

(ii) **J004336.68+410811.8**: This object appears in the GHJ16 sample and is estimated to have a luminosity of $\log(L/L_\odot) = 5.86$. It is also mentioned in the ME16 study as a possible RSG but has no derived luminosity due to the object having no *K*-band photometry. However, the object is resolved in *HST U*-band imaging, showing that it is instead a star cluster. The object was rejected from our sample.

3.4 Sample completeness

Inferring an upper luminosity limit of cool supergiants is difficult due to the steep power law present in the RSG luminosity function, as a result of both the initial mass function (IMF) and the short lifetimes of massive stars. This means low number statistics have a strong influence on our results, as $L_{\rm max}$ is extremely sensitive to sample size (discussed in more detail in Section 4.2.3). Therefore we aim to ensure sample completeness for all RSGs with $\log(L/L_\odot) > 5$, since we are focused on the high end of the RSG luminosity function and the HD limit. Below this luminosity, we are at more risk of including contaminating objects. To aim for completeness, as mentioned in Section 2.1, we cross-checked our sample with other M31 RSG catalogues that instead optically select their RSGs to check that all previously identified RSGs were acquired through our mid-IR cuts. There were, however, a small number of objects that were missing from the Khan catalogue, as previously discussed in Section 3.1, which are located in spatially extended mid-IR emission, meaning that they are not point sources in the mid-IR. Therefore, the only RSGs that could be missed by our sample selection are those that are faint in the optical (e.g. due to circumstellar dust) but also spatially extended in the mid-IR due to confusion with other nearby sources and are hence missing from the point-source catalogue. Any objects that were absent from the mid-IR point-source catalogue but were bright in optical wavelengths were manually added to our sample. All RSG candidates found in the present work that were *also* found in previous studies can be seen in Fig. 5. The total number of RSG candidates that we found in this study is 415, although for the statistical analysis carried out in the present work (see Section 4.2 onward) we take our sample size to be 117, which is the number of RSGs with $\log(L/L_\odot) > 5$.

ME16 has a sample of 251 M31 RSGs with assigned spectral classifications, where 50 of these have a luminosity greater than $\log(L/L_\odot) > 5$. From their sample we have reacquired all 50 of those with $\log(L/L_\odot) > 5$ in our sample.

The total number of RSGs with $\log(L/L_\odot) > 5$ in GHJ16 is 139. We reacquired 128 of these either with our cuts or by manually adding them to our sample if not present in the Khan (2017) catalogue. The remaining 11 objects were inspected in *HST* and SDSS imaging, and in each case we found justification for rejecting them from our sample. The reasons for rejection in each of these 11 individual cases are discussed in Section 3.4.1.

This means that our sample contains all the known RSGs in M31 with $\log(L/L_\odot) > 5$ from previous work as well as 48 candidates that we found through our own colour–magnitude criteria.[2]

3.4.1 Rejected stars from ME16 and GHJ16

Below are the objects from previous M31 RSG catalogues that we have rejected from our study:

(i) **J004105.97+403407.9, J004431.71+415629.1, J003942.43+403203.5, and J003811.56+402358.2**: These objects from GHJ16 have *Gaia* EDR3 proper motions that indicate that they are foreground objects, deviating from M31's proper motion by $\sim$3–4σ.

(ii) **J004303.21+410433.8 and J004052.19+403116.6**: These two objects are present in the GHJ16 sample but have assigned spectral types of B0.5I and B8, respectively (Massey, Neugent & Smart 2016).

(iii) **J004416.28+412106.6 and J004259.31+410629.1**: Although the object J004416.28+412106.6 is described as an RSG candidate in GHJ16, both Massey et al. (2016) and Azimlu, Marciniak & Barmby (2011) classify it as an H II region. It also has a low $B - V$ colour of 0.22, which corresponds to a spectral classification much earlier than K or M. Similarly, J004259.31+410629.1 has a low $B - V$ colour of 0.70, which again suggests an early spectral type. *Gaia* EDR3 also shows J004259.31+410629.1 to have a huge proper motion (19.8 mas yr^{-1}), suggesting that it is not an M31 object. Additionally, Soraisam et al. (2020) discuss that not only is this object located within an H II region, it also shows characteristics of being a W-Ursae-Majoris contact binary, with J004259.31+410629.1 being foreground.

(iv) **J003948.45+403131.5**: This object has a *Gaia* BP − RP colour of 0.73, which means that it does not meet our red criteria. It is absent from the Khan (2017) mid-IR catalogue for M31 due to being spatially extended and has crowded LGGS photometry, which *Gaia* EDR3 is unable to resolve. It is described as a young cluster by Caldwell et al. (2009), Kang et al. (2012) and is therefore rejected from our sample.

(v) **J004331.04+411815.9 and J004336.68+410811.8**: These two objects are both located in the halo of M31 and appear to be spatially extended in *HST* PHAT images, which suggests that they are possibly globular clusters.

4 DISCUSSION

4.1 Comparison with previous work

Our results show that the luminosities determined in the present work are on average lower compared to those found for the same stars in previous work, especially those at the high end of the luminosity function. In particular, for the stars J004539.99+415404.1, J004520.67+414717.3, and J004428.12+415502.9, ME16 find $\log(L/L_\odot) = 5.81$, 5.81, and 5.64, respectively. These are 0.32, 0.06, and 0.11 dex brighter than those found in the present work. The same

[2]It should be noted that, when we calculated the luminosities using our SED method of all the stars from previous work, some had revised luminosities, meaning that they no longer had luminosities greater than $\log(L/L_\odot) > 5$; hence our sample size greater than $\log(L/L_\odot) > 5$ is smaller than that in GHJ16.

Downloaded from https://academic.oup.com/mnras/article/510/3/3132/6445032 by Liverpool John Moores University user on 09 May 2022

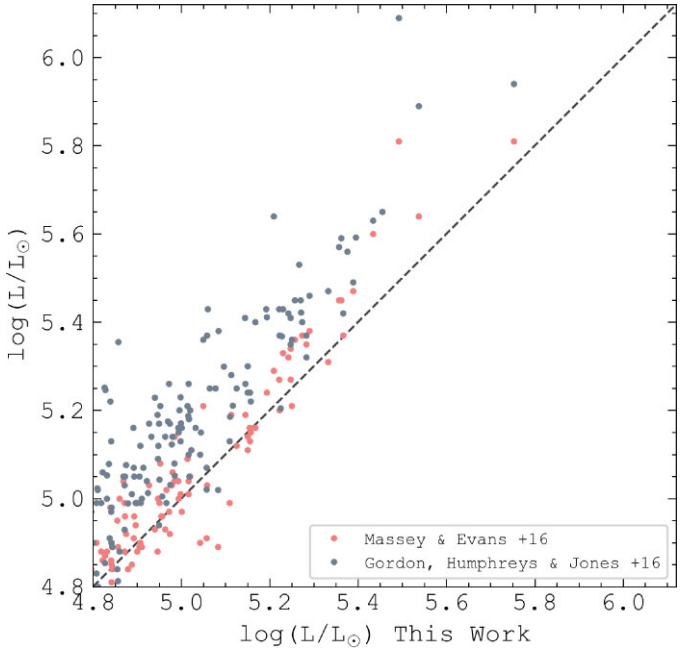

Figure 6. Comparison of bolometric luminosities found in the present work and previous studies of M31 RSGs. The grey points denote the luminosities from this work compared with GHJ16 and the pink points show gthe comparisons of this work with the luminosities from ME16. The black dashed line indicates the 1:1 line.

is seen when compared to GHJ16, where they find log (L/L$_\odot$) values of 6.09, 5.94, and 5.89, which are 0.60, 0.19, and 0.36 dex brighter than those of this work. This is shown in Fig. 6, where there is both a systematic offset between the luminosity samples as well as object-to-object differences. Below we describe the differences between these studies in more detail.

4.1.1 Comparison with ME16 and Neugent et al. (2020)

We find our luminosities to be broadly consistent with those found from ME16; however, there is a disagreement when it comes to the higher-luminosity RSGs. We include comparisons with more recent work by Neugent et al. (2020), who also measure the RSG luminosity function in M31 and adopt a few of the same techniques as ME16, such as the extinction correction method and the use of a BC$_K$ to determine bolometric luminosity. Here we discuss the possible reasons for differences in luminosity for these objects.

First, to correct for foreground visual extinction A_V in ME16, they adopt a uniform value of $A_V = 1$ derived from their spectral fits to optical spectrophotometry of each RSG in their sample. Later work by Neugent et al. (2020) uses the same approach but also introduces a brightness-dependent extinction component that causes the brightest RSGs to have extinctions proportional to their K-band brightnesses. This then has the effect of systematically shifting the brighter RSGs to higher luminosities and warmer temperatures, which leads to a higher L_{max} of log (L/L$_\odot$) $\approx$ 5.7, compared to when adopting a uniform $A_V = 1$, resulting in a reduced L_{max} of approximately log (L/L$_\odot$) $\approx$ 5.5. Though Massey et al. (2021) comment that using this added extinction component leads to 'much better agreement with the evolutionary tracks' than would have occurred by adopting a uniform $A_V = 1$, our goal in the present work is to test these same evolutionary models. Therefore, for us to use these models to inform our choice of extinction correction would be circular logic on our part. Instead, we employ an independent method to estimate each star's extinction, specifically, through the use of an M31 extinction map (Dalcanton et al. 2015) and adopting the median $A_V = 1.19 \pm 0.10$ for those not covered by the map. Therefore, the extinctions that we assign to the brightest objects are inevitably lower than those adopted by Neugent et al. (2020).

To obtain bolometric fluxes, ME16 employ the T_{eff}–BC$_K$ relation, derived from fitting MARCS model atmospheres to optical spectra from Massey et al. (2009). However, it is well known that these model atmospheres perform poorly at optical wavelengths, leading to systematic errors in T_{eff} and BC$_K$ (Davies et al. 2013). Our method of estimating L_{bol} from integrating the SED is free of any such model dependences.

Another factor that directly affects their luminosities is *HST* PHAT and *Gaia* EDR3, showing some of their most luminous RSGs resolving into multiple sources. In the present work, we have flagged that both J004539.99+415404.1 and J004428.12+415502.9 resolve into two objects, both with one source having a proper motion inconsistent with M31 and the other being a likely M31 member. When we account for the luminosity of the blended stars in these cases, it results in a downward revision of the our original SED-derived L_{bol}.

4.1.2 Comparison with GHJ16

The bolometric luminosities calculated for the RSG candidates in GHJ16 are on average 0.16 dex higher than those found for the same stars in the present work. Fig. 6 shows the systematic offset in luminosity between the two studies. In GHJ16, they adopt the same approach of integrating SEDs to obtain L_{bol}, although they only integrate from the optical to the near-IR K band, unless there is evidence for circumstellar dust where they then integrate out to the 22 μm *WISE* band. However, the *WISE* mid-IR photometry has limited angular resolution, which can result in incorrect cross-identification of objects in different catalogues, as highlighted by GHJ16 themselves. An informative example of this is the source J004539.99+415404.1, which appears in the GHJ16 catalogue as

Downloaded from https://academic.oup.com/mnras/article/510/3/3132/6445032 by Liverpool John Moores University user on 09 May 2022

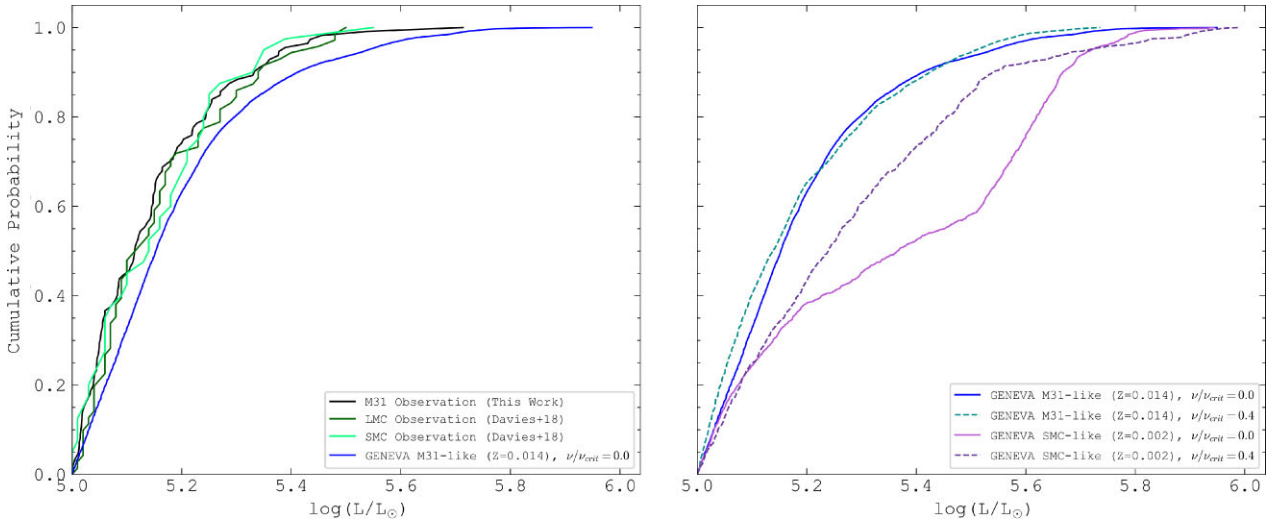

Figure 7. Left: The cumulative luminosity distribution of all the red supergiants with an observational luminosity $\log(L/L_\odot) > 5$ in M31 from this work, as well as for the Large and Small Magellanic Clouds from DCB18. Right: Cumulative luminosity distribution of the cool supergiants with a luminosity $\log(L/L_\odot) > 5$ from the model luminosity functions predicted by Geneva, at both solar (Ekström et al. 2012) and SMC-like (Georgy et al. 2013) metallicities for both the rotating and non-rotating models. We include the 'M31-like' non-rotating model-predicted distribution in the left-hand panel for comparison.

having $\log(L/L_\odot) = 6.09$. In their analysis, GHJ16 employ photometry from the AllWISE catalogue across all four bands. However, inspection of the *WISE* images at 12 and 22 μm reveals that there is no point source at this position. Instead, at these wavelengths we see only the bright background emission of the underlying spiral arm, which is incorrectly attributed to the RSG in the AllWISE point-source catalogue. This phenomenon is responsible for GHJ16 overestimating the luminosities of many objects in their sample.

A second difference between the present work and GHJ16 is how extinction is accounted for. GHJ16 explore two separate methods: first, they estimate A_V from colours of nearby O- and B-type stars; secondly, they derive A_V from the relation between neutral hydrogen column density and the colour excess $E(B-V)$ along the line of sight to each RSG candidate. However, since a large fraction of their RSGs have no nearby OB stars, not all of their RSGs have A_V estimates from both methods, where ~ 67 per cent of their stars have H I-based A_V estimates only. In the circumstances where there is an extinction measurement available via both methods, the OB star method is favoured. However, this method often yields a much larger A_V compared to their alternate method, one example being the RSG candidate J004304.62+410348.4. For this example, they find $\log(L/L_\odot) = 5.40$ with $A_V = 2.1$ from their adopted OB colour method, but they also find $A_V = 1.3$ from the neutral hydrogen column density method. Using these higher extinction values contributes to the higher luminosities for these stars.

4.2 Comparison to lower metallicities

To make a broader test of the metallicity dependence of L_{max} and the luminosity function, we perform two comparisons. First, we compare the empirical luminosity functions of the LMC and SMC with M31. Secondly, we compare the M31 luminosity function and L_{max} to theoretical expectations of lower metallicities using population synthesis.

4.2.1 Observational comparisons between the LMC and SMC

We look at the cumulative RSG luminosity function for M31 and compare it with the empirical SMC and LMC distributions from DCB18, looking at all RSGs with $\log(L/L_\odot) > 5$, where our sample is considered to be complete. In these galaxies, the metallicities are thought to be $\sim$0.25Z$\odot$ and 0.5Z$\odot$, respectively (Russell & Dopita 1990). As noted previously, we assume that the M31 metallicity lies in the range of 1.06–1.66Z$\odot$ (Zurita & Bresolin 2012). The left-hand panel of Fig. 7 shows the similarities of the observed cumulative luminosity functions for M31, SMC, and LMC. We perform a Kolmogorov–Smirnov (KS) test to evaluate these similarities by measuring the differences between the cumulative distribution functions. For the empirical M31 distribution compared with the SMC and LMC, we find a 60 per cent and 44 per cent probability, respectively, that they are drawn from the same parent distribution. Hence, the probability that the RSG luminosity functions in the three galaxies are consistent with one another is within 1σ. Furthermore, each galaxy has the same L_{max} to within 0.1 dex at $\log(L/L_\odot) \sim 5.5$. Therefore, we find no evidence that the luminosities of RSGs have a dependence on metallicity. In the next section, we will compare these empirical findings to theoretical predictions.

4.2.2 Theoretical predictions of the luminosity distribution

To compare our observational results to theoretical predictions, we perform a population synthesis analysis. We do so by first generating a sample of random initial masses between 8 and 60M$_\odot$ according to the Salpeter initial mass function (IMF). Each star is randomly assigned an age between 0 and 38 Myr, under the implicit assumption of a constant star-formation rate. We then match these to evolutionary tracks using SYnthetic CLusters Isochrones & Stellar Tracks (SYCLIST) from the Geneva group at solar metallicity ($Z = 0.014$) (Ekström et al. 2012), to interpolate L_{bol} and T_{eff} from the track of each simulated star, removing any stars with ages greater than the star's maximum expected lifetime. We also apply a temperature cut at $\log T_{eff} < 3.8$ to ensure that the sample consists of cool supergiants. We perform a Monte Carlo experiment where we draw a random sample of stars from the model population, matching the observed number of RSGs in M31, and show the mean number of stars in each luminosity bin for both the rotating and non-rotating models.

Downloaded from https://academic.oup.com/mnras/article/510/3/3132/6445032 by Liverpool John Moores University user on 09 May 2022

The result is a simulated luminosity distribution for a constant star-formation rate.

The comparison of this simulated distribution to the observations shows that the model perhaps slightly overpredicts the number of luminous stars at the high end of the distribution compared to observation for M31, but, more notably, predicts $L_{\rm max}$ to be much higher than we observe. However, at the high-luminosity end we do have a very small sample size and so our results are subject to stochastic uncertainties, which we will quantify in Section 4.2.3.

The right-hand panel of Fig. 7 shows the model cumulative RSG luminosity functions at M31-like metallicity for both the rotating and non-rotating models. It can be seen that, although the shapes of the M31 cumulative distributions are quite similar, there is a distinct difference in $L_{\rm max}$, where the non-rotating models predict a higher maximum luminosity compared to the rotating models. When compared to the observed M31 cumulative distribution in the left-hand panel of Fig. 7, there is a clear difference between the model and observed distributions.

When we take a look at the model cumulative luminosity function of RSGs at SMC-like ($Z = 0.002$) metallicity (SMC-like tracks are from Georgy et al. 2013), seen in the right-hand panel of Fig. 7, there is not only a clear difference between the distributions of the rotating and non-rotating models, but a distinct contrast between the model M31 and model SMC distributions. Therefore, the models predict that we should see a difference between the RSG luminosity functions of M31 and the SMC. However, despite the contrast in metallicity, the observed RSG cumulative distributions are consistent with each other to within 1σ, as shown previously in Section 4.2.1.

We now compare the observational and model-predicted M31 and SMC-like cumulative distributions using a KS test, as in the previous section. Here we find a probability of 5 per cent (rotating) and 0.1 per cent (non-rotating) for the M31 models compared with observations and a 0.02 per cent (rotating) and 10^{-6} per cent (non-rotating) probability for the SMC models compared with observations. These low probabilities lead us to conclude that there is little similarity between the model distributions in the two galaxies and they are unlikely to be drawn from the same parent distribution. This is in sharp contrast to what we see in the empirical distributions of M31 and the SMC, which are statistically indistinguishable.

4.2.3 *Comparisons to theoretical predictions of* L_{max}

From our observational study of the M31 RSG population, as previously discussed, after the marginal candidate J004520.67+414717.3 with $\log(L/L_\odot) = 5.75 \pm 0.11$, the next five most luminous stars span the range of $5.43 < \log(L/L_\odot) < 5.53$, suggesting an upper luminosity limit for M31 of $\log(L/L_\odot) \approx 5.5$. In this section, we take a closer look at the statistical significance of $L_{\rm max}$ at M31 and SMC-like metallicities as predicted from the Geneva models.

By simply looking at the parameter space occupied by the evolutionary tracks on an HR diagram, the Geneva models predict that $L_{\rm max}$ for M31 should be in the range $5.7 \lesssim \log(L/L_\odot) \lesssim 5.8$, yet we observe a much lower limit of $\approx$5.5. However, we are dealing with small number statistics at the high-luminosity end. This results in stochastic effects where the $L_{\rm max}$ that we observe is a function of our sample size, meaning the larger the sample size, the higher the probability of sampling close to the true HD limit. Therefore, when comparing model predictions to observations, we must be careful to take this effect into account.

To investigate the effects of sample size on $L_{\rm max}$, we perform another Monte Carlo experiment where we randomly select N stars from the theoretical luminosity function and determine $L_{\rm max}$ of that sample. We repeat this 10^5 times to find the average $L_{\rm max}$ for each sample size of N cool supergiants with $\log(L/L_\odot) > 5$. The results of this are shown in Fig. 8 for both M31 and SMC-like metallicities. It shows the $L_{\rm max}$ that we would expect to measure, plus the confidence intervals of that value, as a function of sample size. As one would expect, larger sample sizes result in the higher-luminosity bins being more populated, meaning that the $L_{\rm max}$ that we observe is more likely to reflect the 'true' $L_{\rm max}$, with a smaller associated uncertainty.

In each panel of Fig. 8, the empirical $L_{\rm max}$ for the sample size that we observe for that galaxy is denoted by the black star. Although M31 shows agreement within 3σ, the SMC shows a disagreement beyond the 99.7 per cent confidence limit. This increasing disagreement between observations and theoretical predictions as a function of metallicity can be understood as follows: As shown earlier, the empirical $L_{\rm max}$ is observed to be metallicity invariant. By contrast, the theoretical expectation of $L_{\rm max}$ in single-star evolution is governed by metallicity-dependent mass-loss and so increases with decreasing Z.

In summary, we find no significant difference in $L_{\rm max}$ within the errors across a metallicity baseline of ($0.25 Z_\odot$ to $\gtrsim Z_\odot$). This is in clear disagreement with theoretical expectations because $L_{\rm max}$ predictions from the models are simply too high compared to observational measurements and this effect is predicted to only increase with decreasing metallicity.

4.3 Possible explanations for a metallicity-invariant HD limit

The results of this work have shown that the observational luminosity function of RSGs does not follow theoretical expectations, in terms of both $L_{\rm max}$ and the shape of the luminosity function. There are several well known sources of uncertainty in stellar evolutionary models, particularly in the pre-supernova phases of massive stars, such as mass-loss, mixing processes, and rotational effects. In the present section, we discuss the possible implications that these parameters may have for the theoretical predictions of the HD limit.

4.3.1 *Mass-loss*

Mass-loss is a key process responsible for the stripping of the hydrogen envelopes of stars. Hot star winds on the MS are driven by radiation pressure due to metal absorption lines in the UV, which means that wind strength is sensitive to metallicity. It is this dependence of wind strength on metallicity that results in the predicted metallicity dependence of the HD limit in single-star models. However, it has been seen from the cumulative luminosity functions of the RSGs in M31, LMC, and SMC and from the invariance of $L_{\rm max}$ across these galaxies that there is no metallicity dependence. Also, recent work has shown that the mass-loss rates from these metallicity-dependent hot star winds are being revised downward by a factor of $\sim$3 (e.g. Sundqvist et al. 2019; Björklund et al. 2021), and so they are even less effective at removing the hydrogen envelope than previously thought. Therefore, we conclude that line-driven winds in the hot star phases *cannot* be the cause of the HD limit.

We next take a look at the contribution of mass-loss as a result of RSG winds, for which there is some evidence to suggest that more metal-poor environments result in weakened RSG wind speeds (e.g. Goldman et al. 2017). The most widely used RSG wind prescription in stellar evolutionary codes is from de Jager, Nieuwenhuijzen & van der Hucht (1988), but this is thought to overestimate the rate of mass-loss ($\dot{M}$), particularly for more luminous RSGs, as discussed

Downloaded from https://academic.oup.com/mnras/article/510/3/3132/6445032 by Liverpool John Moores University user on 09 May 2022

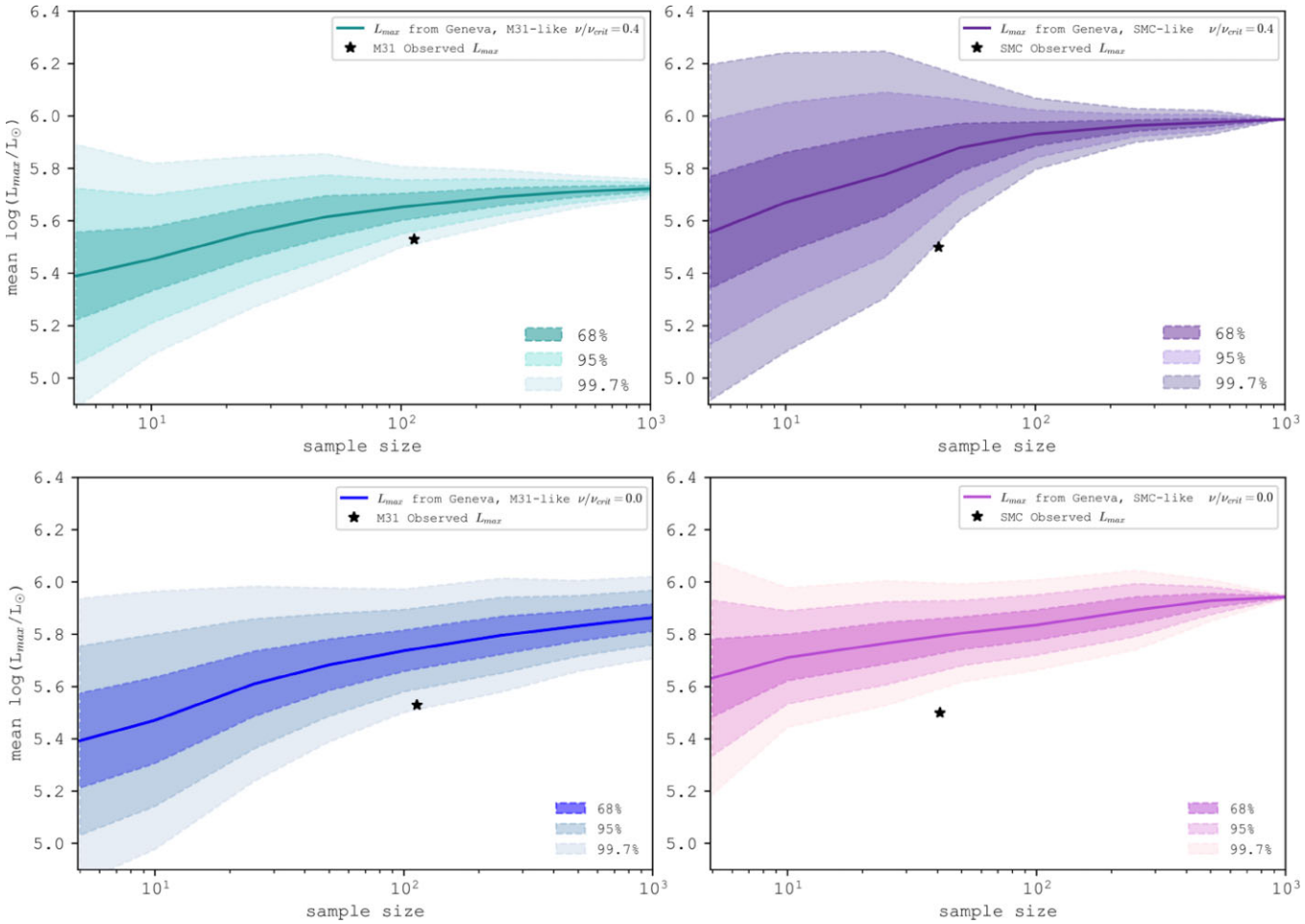

Figure 8. The expected $L_{\rm max}$ for a range of sample sizes as predicted by the Geneva rotating models for both solar ($Z = 0.014$) and SMC-like ($Z = 0.002$) metallicities. The shaded regions indicate the confidence limits on $L_{\rm max}$ as shown in the legend and the black stars indicate the observed $L_{\rm max}$ and sample size for M31 from this work and the same for the SMC from DCB18.

in Beasor et al. (2020). A new RSG $\dot{M}$ prescription, presented in the latter study, implies that only a small fraction of envelope mass is lost during the RSG phase ($\sim$1M$_{\odot}$). This is considerably lower than that with the prescription implemented in the Geneva models, in which up to $\sim$50 per cent of the envelope mass can be lost during this period. In fact, with the Beasor et al. (2020) mass-loss recipe implemented instead, higher-mass stars (>30M$_{\odot}$) no longer evolve back to the bluer side of the HR diagram, resulting in a larger number of higher-mass stars remaining in the RSG phase. Therefore, despite offering a more accurate description of $\dot{M}$ for cool supergiants in stellar models, in regard to the HD limit the disagreement actually worsens, giving rise to an even greater upper limit of log (L/L$_{\odot}$) $\sim$ 6. This means that RSG winds are simply not strong enough to be responsible for the HD limit.

The lack of metallicity dependence means that line-driven winds cannot be responsible for the HD limit. However, this does not rule out the episodic-type mass-loss seen in luminous blue variables (LBVs). LBV eruptive mass-loss is so strong that the winds become optically thick and are likely to be driven by continuum radiation pressure in super-Eddington phases. Since we observe LBV eruptions at high and low metallicities, LBV mass-loss is not metallicity dependent (Smith & Owocki 2006). This means we cannot rule out mass-loss from LBV-type eruptions as a potential cause of the HD limit. Similarly, Kraus et al. (2015) suggest that stars in the B[e] supergiant phase are also thought to eject large amounts of material, much like LBVs, which could be another possible type of mass-loss contributing to the HD limit.

Further, it has been argued that the origin of LBV-type eruptions could be a consequence of binary interaction and mergers (e.g. Smith 2014), which could also be an explanation for the existence of the HD limit (see the next section).

4.3.2 *Binarity*

Thus far, in seeking to understand the RSG populations across the three galaxies, we have exclusively considered single-star evolutionary models. However, it is becoming increasingly clear that such models are of limited relevance for the most massive stars. Several studies in the literature have concluded that the fraction of OB stars in binary systems are in the range of 50–60 per cent or higher (Sana et al. 2012, 2013; Dunstall et al. 2015). Furthermore, the probability of a star being in a multiple *and* that the star will interact with this companion appears to increase with increasing mass (Duchêne & Kraus 2013; Moe & Di Stefano 2017). This is also suggested in the recent work of Bodensteiner et al. (2021), who find that the bias-corrected close binary fraction of the $\sim$40 Myr old massive SMC open cluster, NGC 330, is 34^{+8}_{-7} per cent. This is a lower fraction compared to younger clusters in the Milky Way and LMC. For

Downloaded from https://academic.oup.com/mnras/article/510/3/3132/6445032 by Liverpool John Moores University user on 09 May 2022

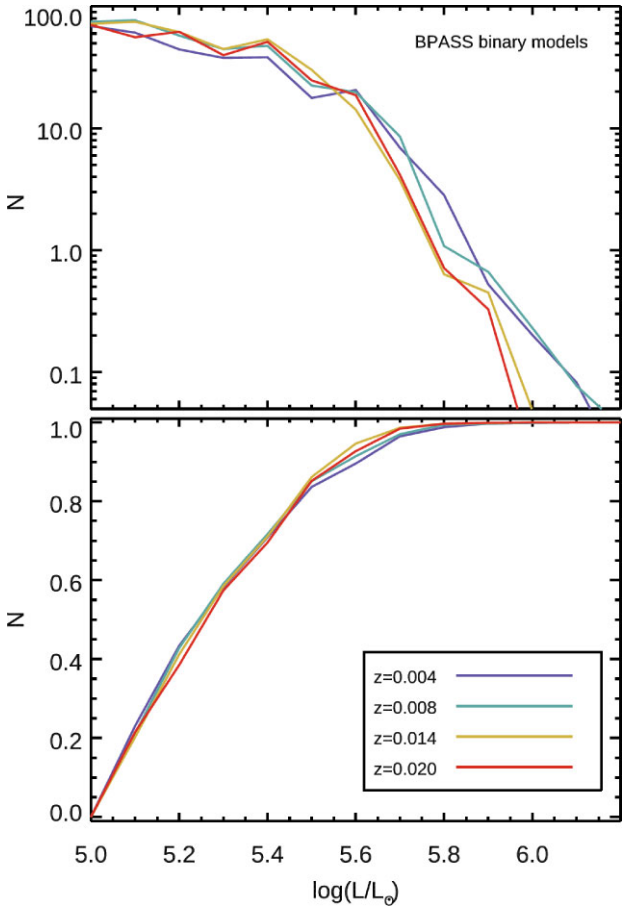

Figure 9. Top: Predictions of the luminosity function of cool supergiants from BPASS binary population synthesis for the metallicity range $Z = 0.004$–0.020. Bottom: The same result but shown as a cumulative luminosity distribution.

example, the Cygnus OB2 association within our Galaxy has an intrinsic binary fraction of ≈55 per cent (Kobulnicky et al. 2014). The counterpart fraction for the overall B-star population of the LMC 30 Doradus region is found to be 58 ± 11 per cent (Dunstall et al. 2015). This means that, above some mass threshold, it is reasonable to expect that the likelihood of a star evolving according to single stellar evolutionary tracks will eventually tend towards zero. Specifically, a star's evolution to the red will be prevented by interaction with a companion either in or before the Hertzsprung gap. This means that we would expect binary effects to also contribute to the mass lost during a star's life; this is therefore a possible explanation for the reduced L_{max} that we see in observations (DCB18).

To investigate the effects of binarity on L_{max}, we extracted the RSG luminosity function for a constant star-formation history from the Binary Population and Spectral Synthesis (BPASS) models. These models assume the mass ratio and period distributions from Moe & Di Stefano (2017), which specify that stars with masses relevant for RSGs ($M > 9M_{\odot}$) have close binary frequencies in excess of 80 per cent. The BPASS RSG luminosity functions as a function of Z are shown in Fig. 9. We still see a metallicity dependence and very high L_{max}, similar to single-star models, in the metallicity range $Z = 0.004$–0.020.

Given the very high close binary fraction for massive stars set within the BPASS simulations, one would expect that most, if not all, of these stars would interact prior to the primary reaching the RSG phase. It is therefore intriguing that the BPASS-simulated RSG luminosity functions behave so similarly to those of the single-star evolution models. In the future, it would be of interest to further mine the BPASS results to investigate the histories of the RSGs in these simulations.

5 CONCLUSIONS

We have compiled a sample of mid-IR selected cool supergiants to measure the luminosity function of the RSG population in M31 to investigate the Humphreys–Davidson limit (L_{max}).

(i) We find that the luminosity function of RSGs is independent of metallicity, based on the range of metallicities studied here (from SMC-like to M31-like).

(ii) L_{max} is also independent of metallicity, where we find that the HD limit for M31 is $\log(L/L_{\odot}) = 5.53 \pm 0.03$, within 0.1 dex of the SMC and LMC. We are in agreement with DCB18, who find a lack of evidence for a metallicity-dependent L_{max}. This suggests that mass-loss from line-driven winds is *not* the cause of the HD limit.

(iii) A population synthesis analysis shows that the single-star Geneva evolutionary models not only overpredict the number of luminous cool supergiants at the high-luminosity end, but also overpredict L_{max}, particularly at lower metallicities.

ACKNOWLEDGEMENTS

The authors would like to thank the referee for their useful comments. SLEM thanks Nathan Smith, Gemma González-Torà, and Tom Sedgwick for useful comments and insightful conversations. SLEM acknowledges support from an STFC studentship, jointly supported by the Faculty of Engineering and Technology at the Astrophysics Research Institute at Liverpool John Moores University. ERB is supported by NASA through Hubble Fellowship grant *HST*-HF2-51428 awarded by the Space Telescope Science Institute, which is operated by the Association of Universities for Research in Astronomy, Inc., for NASA, under contract NAS5-26555. This research has made use of the IDL software ASTROLIB, MATPLOTLIB (Hunter 2007), NUMPY (van der Walt, Colbert & Varoquaux 2011), and SCIPY (Virtanen et al. 2020), as well as the VizieR catalogue access tool and the SIMBAD/ALADIN Sky Atlas operated at CDS, Strasbourg, France (Ochsenbein, Bauer & Marcout 2000; Wenger et al. 2000; Boch & Fernique 2014).

6 DATA AVAILABILITY

The data underlying this article will be shared on reasonable request to the corresponding author. The data sets were derived from sources in the public domain:

(i) LGGS:
cdsarc.unistra.fr/viz-bin/cat/J/AJ/152/62
(ii) *Gaia* EDR3:
cdsarc.unistra.fr/viz-bin/cat/I/350
(iii) 2MASS:
cdsarc.unistra.fr/viz-bin/cat/II/246
(iv) *Spitzer* M31 point-source survey:
cdsarc.unistra.fr/viz-bin/cat/J/ApJS/228/5

REFERENCES

Abbott D. C., 1982, ApJ, 259, 282

Downloaded from https://academic.oup.com/mnras/article/510/3/3132/6445032 by Liverpool John Moores University user on 09 May 2022

Azimlu M., Marciniak R., Barmby P., 2011, AJ, 142, 139
Beasor E. R., Davies B., Smith N., van Loon J. T., Gehrz R. D., Figer D. F., 2020, MNRAS, 492, 5994
Björklund R., Sundqvist J. O., Puls J., Najarro F., 2021, A&A, 648, A36
Boch T., Fernique P., 2014, in Manset N., Forshay P., eds, ASP Conf. Ser. Vol. 485, Astronomical Data Analysis Software and Systems XXIII. Astron. Soc. Pac., San Francisco, p. 277
Bodensteiner J. et al., 2021, A&A, 652, A70
Brunish W. M., Gallagher J. S., Truran J. W., 1986, AJ, 91, 598
Caldwell N., Harding P., Morrison H., Rose J. A., Schiavon R., Kriessler J., 2009, AJ, 137, 94
Cardelli J. A., Clayton G. C., Mathis J. S., 1989, ApJ, 345, 245
Castor J. I., Abbott D. C., Klein R. I., 1975, ApJ, 195, 157
Courteau S., Widrow L. M., McDonald M., Guhathakurta P., Gilbert K. M., Zhu Y., Beaton R. L., Majewski S. R., 2011, ApJ, 739, 20
Cutri R. M. et al., 2003, 2MASS All Sky Catalog of Point Sources
Dalcanton J. J. et al., 2012, ApJS, 200, 18
Dalcanton J. J. et al., 2015, ApJ, 814, 3
Davies B., Beasor E. R., 2018, MNRAS, 474, 2116
Davies B., Beasor E. R., 2020, MNRAS, 493, 468
Davies B. et al., 2013, ApJ, 767, 3
Davies B, Crowther P. A., Beasor E. R., 2018, MNRAS, 478, 3138 (DCB18)
de Jager C., Nieuwenhuijzen H., van der Hucht K. A., 1988, A&AS, 72, 259
Duchêne G., Kraus A., 2013, ARA&A, 51, 269
Dunstall P. R. et al., 2015, A&A, 580, A93
Ekström S. et al., 2012, A&A, 537, A146
Ferrari A., Galeotti P., Silvestro G., Trussoni E., 1970, Ap&SS, 9, 181
Gaia Collaboration et al., 2020, A&A, 649, A1
Georgy C. et al., 2013, A&A, 558, A103
Goldman S. R. et al., 2017, MNRAS, 465, 403
Gordon M. S., Humphreys R. M., Jones T. J., 2016, ApJ, 825, 50 (GHJ16)
Humphreys R. M., 1983, ApJ, 265, 176
Humphreys R. M., Davidson K., 1979, ApJ, 232, 409
Hunter J. D., 2007, Comput. Sci. Eng., 9, 90
Kang Y., Rey S.-C., Bianchi L., Lee K., Kim Y., Sohn S. T., 2012, ApJS, 199, 37
Karachentsev I. D., Karachentseva V. E., Huchtmeier W. K., Makarov D. I., 2004, AJ, 127, 2031
Khan R., 2017, ApJS, 228, 5
Kobulnicky H. A. et al., 2014, ApJS, 213, 34
Kraus M., Oksala M. E., Cidale L. S., Arias M. L., Torres A. F., Borges Fernandes M., 2015, ApJ, 800, L20
Kudritzki R.-P., 2003, A Massive Star Odyssey: From Main Sequence to Supernova, 212, 325
Kudritzki R. P., Pauldrach A., Puls J., 1987, A&A, 173, 293
Lamb S. A., Iben I. J., Howard W. M., 1976, ApJ, 207, 209
Maeder A., 1981, A&A, 102, 401
Maeder A., Meynet G., 2003, A&A, 411, 543
Massey P., Evans K. A., 2016, ApJ, 826, 224 (ME16)
Massey P., Olsen K. A., Hodge P. W., Jacoby G. H., McNeill R. T., Smith R. C., Strong S. B., 2006, BAAS, 38, 939
Massey P., Silva D. R., Levesque E. M., Plez B., Olsen K. A. G., Clayton G. C., Meynet G., Maeder A., 2009, ApJ, 703, 420
Massey P., Neugent K. F., Smart B. M., 2016, AJ, 152, 62
Massey P., Neugent K. F., Levesque E. M., Drout M. R., Courteau S., 2021, AJ, 161, 79
Moe M., Di Stefano R., 2017, ApJS, 230, 15
Neugent K. F., Massey P., Georgy C., Drout M. R., Mommert M., Levesque E. M., Meynet G., Ekström S., 2020, ApJ, 889, 44
Ochsenbein F., Bauer P., Marcout J., 2000, A&AS, 143, 23
Rieke G. H., Lebofsky M. J., 1985, ApJ, 288, 618
Rodrigo C., Solano E., 2020, Contr. XIV.0 Scientific Meeting (virtual) of the Spanish Astron. Soc. Sea Astronima, Spain, p. 182
Russell S. C., Dopita M. A., 1990, ApJS, 74, 93
Salomon J. B., Ibata R., Reylé C., Famaey B., Libeskind N. I., McConnachie A. W., Hoffman Y., 2020, MNRAS, 507, 2592
Sana H. et al., 2012, Science, 337, 444
Sana H. et al., 2013, A&A, 550, A107
Sandage A., Tammann G. A., 1974, ApJ, 191, 603
Smith N., 2014, ARA&A, 52, 487
Smith N., Owocki S. P., 2006, ApJ, 645, L45
Soraisam M. D. et al., 2018, ApJ, 859, 73
Soraisam M. D., Bildsten L., Drout M. R., Prince T. A., Kupfer T., Masci F., Laher R. R., Kulkarni S. R., 2020, ApJ, 893, 11
Stothers R., 1969, ApJ, 155, 935
Stothers R., Chin C. W., 1978, ApJ, 226, 231
Stothers R., Chin C. W., 1979, ApJ, 233, 267
Sundqvist J. O., Björklund R., Puls J., Najarro F., 2019, A&A, 632, A126
Tempel E., Tamm A., Tenjes P., 2010, A&A, 509, A91
van der Walt S., Colbert S. C., Varoquaux G., 2011, Comput. Sci. Eng., 13, 22
van Loon J. T., Cioni M. R. L., Zijlstra A. A., Loup C., 2005, A&A, 438, 273
Vink J. S., de Koter A., Lamers H. J. G. L. M., 2001, A&A, 369, 574
Virtanen P. et al., 2020, Nat. Methods, 17, 261
Wenger M. et al., 2000, A&AS, 143, 9
Wirth A., Smarr L. L., Bruno T. L., 1985, ApJ, 290, 140
Zurita A., Bresolin F., 2012, MNRAS, 427, 1463

This paper has been typeset from a TEX/LATEX file prepared by the author.

Downloaded from https://academic.oup.com/mnras/article/510/3/3132/6445032 by Liverpool John Moores University user on 09 May 2022